Graphene-Coated Two-Layer Dielectric Loaded Surface Plasmon Polariton Rib Waveguide with Ultra-Long Propagation Length and Ultra-High Electro-Optic Wavelength Tuning

Tao Ma[1], Jinhui Yuan[2,3], (Senior Member, IEEE), Fang Wang[1], Heng Liu[1], Xian Zhou[3], Keping Long[3], (Senior Member, IEEE), Chongxiu Yu[2], and Yufang Liu[4]

[1]Henan Key Laboratory of Optoelectronic Sensing Integrated Application, College of Electronic and Electrical Engineering, Henan Normal University, Xinxiang 453007, China

[2]State Key Laboratory of Information Photonics and Optical Communications, Beijing University of Posts and Telecommunications (BUPT), Beijing 100876, China

[3]Research Center for Convergence Networks and Ubiquitous Services, University of Science & Technology Beijing (USTB), Beijing 100083, China

[4]School of Physics, Henan Normal University, Xinxiang 453007, China

Corresponding author: Jinhui Yuan (e-mail: yuanjinhui81@bupt.edu.cn).

ABSTRACT A graphene-coated two-layer dielectric loaded surface plasmon polariton (GTDLSPP) rib waveguide is designed. The mode characteristics and electro-optic (EO) modulation performances of the four hybrid plasmonic modes (HPMs) in the designed waveguide are simulated by using the finite element method. The simulation results show that a 10^3 mm-scale propagation length and an effective mode field area of $\sim\lambda^2/1333$ are obtained by adjusting the bias voltage. The EO wavelength tunings are -68.6, -42.0, -49.7, and -11.1 nm/V for the HPM 1, HPM 2, HPM 3, and the peak 2 of HPM 4, which are two orders of magnitude larger than those of other EO modulation structures. For the peak 1 of the HPM 4, the EO wavelength tuning is the piecewise linear. For a 150-μm long waveguide, the modulation depths of $\sim$98.7, $\sim$87.9, and 99.5%, and FWHMs of $\sim$450, $\sim$100, and $\sim$42 nm can be achieved for the HPM 1, HPM 2, and HPM 3. For the HPM 4, there are two peaks in the transmission spectrum. The modulation depths are $\sim$97.3 and 75.2%, and FWHMs are $\sim$92 and $\sim$34 nm for the peaks 1 and 2. There is a tradeoff between the modulation depth and FWHM for different waveguide lengths. The GTDLSPP rib waveguide designed has small size, high modulation depth, broad bandwidth, and compatibility with the CMOS technology, so it has potential applications in the EO tunable devices, optical interconnects, and optical switches.

INDEX TERMS Surface plasmon polariton waveguide, Electro-optic modulation, Graphene,

I. INTRODUCTION

The development of integrable optical signal processing technology requires ultra-compact on-chip photonic devices and systems [1]. As one of the most critical devices, electro-optic (EO) modulator, which can manipulate the different parameters of light, should have broad bandwidth, low energy consumption, low insertion loss, and good compatibility with the complementary metal oxide semiconductor (CMOS) technology. At present, the modulators based on thermo-optic [2], electro-absorption

[3], magneto-optic [4], reflection structure [5], and all-optical technology [6] have been widely investigated.

Graphene as a promising 2D material provides the impetus for the high-speed photonic system due to its superior properties, including high gate-variable carrier mobility at room temperature, broadband operation, strong graphene-light interaction, ultra-high thermal conductivity, ultra-fast saturable absorption [7]. Moreover, the Fermi energy of graphene can be adjusted by the electrical gating [8], which can convert the electric data to the optical signals [9]. Therefore, the graphene-based EO modulators have been

attracting great research interests [10]. However, the interaction between the graphene and vertical incident light becomes weak due to the atomic thickness of the graphene. In order to enhance the interaction, the modulators based on Mach-Zehnder interferometer [11], integrated optical cavities [12, 13], patterned graphene structures [14, 15], hybrid plasmonic structures [16, 17] have been demonstrated. Among them, the graphene-on-silicon (GoS) waveguides show excellent characteristics owing to the advantages of graphene [18, 19].

For the optical devices based on silicon-on-insulator (SOI) waveguides, high integration density and miniaturization remain major challenges in micro and nanotechnology due to the diffraction limit [20]. In contrast, the plasmonic waveguides can break the diffraction limit and achieve the subwavelength optical confinement at the interface between the dielectric and metal [21]. Thus, the hybrid plasmonic waveguides (HPWs), which combine the two or more types of waveguides into a single structure, are widely used as the compact modulators. The HPW can generate the hybrid modes to improve the compromise losses and confinement [22], and provide a scheme for the enhanced EO modulation at a small length scale [23]. Recently, the graphene plasmonic waveguide, which is also called as graphene HPW (GHPW), has been demonstrated to guide the surface plasmon polariton (SPP) wave [24]. The GHPW-based modulators combine the advantages of the graphene and plasmonic waveguides. However, the combination of the graphene and plasmonic waveguides presents a challenge due to the anisotropy permittivity of the graphene [25], which could be improved by optimizing the design of an engineered device. A GHPW composed of a Si-graphene-SiO$_2$ sandwich and a silver cylindrical nanowire is designed for the EO modulation, whose modulation depth is ~0.3 dB·μm^{-1} at low gating voltages [26]. Moreover, the GHPW is combined with a metal-insulator-metal (MIM) structure, which can increase the modulation depth to ~0.6 dB·μm^{-1}. To manipulate the angular momentum of photons at the THz frequency, a GHPW based on a gallium arsenide (GaAs) waveguide embedded in high-density polyethylene (HDPE) with five-layer graphene is proposed [27]. The relative phase of π/2 is achieved when the graphene length is 145 μm. A chain of three metal disks on a GHPW is used to realize a submicron EO modulator, whose extinction ratio (*ER*) is 5.5 dB, waveguide length is 740 nm, and 3-dB bandwidth is 83.4 GHz at wavelength 1.55 μm [28]. To enlarge the bandwidth, a graphene-based plasmonic valley-slot waveguide modulator is presented [29]. A GHPW modulator based on graphene-hexagonal-boron-nitride-graphene sandwich is analyzed [30], where the modulator has a high *ER* of 39.75 dB and a large bandwidth of 190.5 GHz. By optimizing the parameters, a modulation depth of 3 dB is achieved within a broad wavelength range from 1400 to 1600 nm. A graphene sheet as an absorber tunable layer is embedded inside a sub-wavelength-thick multilayer structure, which is compose of Ag, Si$_3$N$_4$, and Ta$_2$O$_5$ layers [31]. The modulation depth is 7.5 % at wavelength 1.55 μm. A graphene intensity/phase modulator based on ultra-thin (<80 nm) silicon strip waveguide is designed to improve the modulation efficiency [32]. The modulation depth of 0.280 dB·μm^{-1} with a bandwidth of 216 GHz at a waveguide thickness of 30 nm is achieved. Silicon nitride (Si$_3$N$_4$) waveguide has low propagation loss, relatively small refractive index (RI) contrast, large bandgap, and compatibility with the CMOS process [33]. Thus, it is considered as an ideal candidate for building the optical modulators [34].

In this paper, by combining the advantages of the GHPW, Si$_3$N$_4$, and two-layer dielectric loaded surface plasmon polariton (TDLSPP) waveguide, we propose a graphene-coated two-layer dielectric loaded surface plasmon polariton (GTDLSPP) rib waveguide. Two dielectric layers of the GTDLSPP rib waveguide are silicon and Si$_3$N$_4$, respectively. The mode characteristics and EO tunability of the GTDLSPP rib waveguide are analyzed and optimized. The ultra-long propagation length and ultra-high electro-optic tuning can be achieved. The GTDLSPP rib waveguide can be used as the EO modulator by applying the low bias voltage, which has potential applications in the ultra-compact on-chip micro-nano photonic system. The rest of this paper is organized as follows. In Section II, the structure of the GTDLSPP rib waveguide is designed. In Section III, the mode characteristics of the GTDLSPP rib waveguide are analyzed and optimized. In Section IV, the EO wavelength tuning and modulation performances of the GTDLSPP rib waveguide with the different bias voltage are investigated. Conclusions are drawn in Section V.

II. STRUCTURE DESIGN OF THE GTDLSPP RIB WAVEGUIDE

The schematic of the designed GTDLSPP rib waveguide is shown in Fig. 1. The GTDLSPP rib waveguide consists of a TDLSPP rib waveguide and a monolayer graphene. The GTDLSPP rib waveguide is made of two dielectric layers with different refractive indices (RIs) deposited on a 70-nm thick gold film. The upper layer is the silicon with a high RI of 3.45, and the middle layer is the silicon nitride with a low RI of 2. The cross-section of the GTDLSPP rib waveguide is shown in Fig. 1(b). The thicknesses of the rectangular and rib waveguides are h_1, h_2, and h_3, the length of the waveguide coated with graphene is L_G, and the ridge width of the GTDLSPP rib waveguide is w=500 nm. h_{Au} and g_0 are the thicknesses of the gold film and monolayer graphene, respectively. The substrate and upper cladding of the GTDLSPP waveguide are the silica and air, respectively.
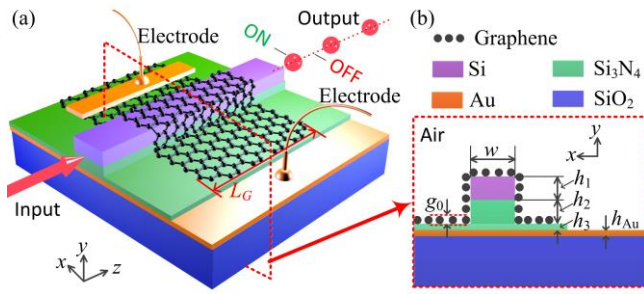
FIGURE 1. (a) Schematic of the designed GTDLSPP rib waveguide, and (b) the corresponding cross-section.

The frequency-dependent relative permittivity of Au can be described by the Drude model [35]

$$\varepsilon_{Au} = \varepsilon_\infty - \frac{\omega_p^2}{\omega(\omega + i\gamma)}, \quad (1)$$

where ε_∞ is the dielectric constant at the infinite frequency, γ is the electron collision frequency, ω_p is the bulk plasma frequency, $\omega = 2\pi/\lambda$ is the angular frequency of the incident light in the vacuum, and λ is the wavelength. For Au, $\varepsilon_\infty = 9.75$, $\omega_p = 1.36 \times 10^{16}$ rad/s, and $\gamma = 1.45 \times 10^{14}$ rad/s [36].

The relative permittivity of the graphene can be equivalently expressed as $\varepsilon_g = 1 + i\sigma_g/(\omega\varepsilon_0 g_0)$ [37], where ε_0 is the permittivity of the vacuum. For the monolayer graphene, g_0 is set as 1 nm. σ_g is the complex conductivity of the monolayer graphene, and can be described as $\sigma_g = \sigma_{intra} + \sigma_{inter}$. σ_{intra} and σ_{inter} correspond to the intraband electron-photon scattering and interband transition contribution, which can be characterized by the Kubo formula [35, 38]

$$\sigma_{intra} = \frac{ie_0^2 k_B T}{\pi\hbar^2(\omega + i\tau^{-1})}[\frac{E_F}{k_B T} + 2\ln(e^{\frac{-E_F}{k_B T}} + 1)], \quad (2)$$

$$\sigma_{inter} = \frac{ie_0^2}{4\pi\hbar}\ln\left[\frac{2E_F - \hbar(\omega + i\tau^{-1})}{2E_F + \hbar(\omega + i\tau^{-1})}\right], \quad (3)$$

where e_0, $\hbar$, and k_B are the electron charge, reduced Plank's constant, and Boltzman's constant, respectively. $T = 300$ K is the temperature in Kelvin. τ^{-1} is the free carrier scattering rate, which is chosen as 2×10^{12} s^{-1} [35]. E_F is the Fermi energy (chemical potential), which can be electrically controlled by the bias voltage supplied to the monolayer graphene. In Eq. (2), at room temperature, E_F is an experimentally tunable parameter, and can be modified by the applied bias voltage as the following equation [39]

$$E_F = \hbar v_F \sqrt{\pi a |V_g|}, \quad (4)$$

where $v_F = 10^6$ m/s is the Fermi velocity, a is the capacitance per unit area per charge, and V_g is the applied bias voltage between the electrodes. To demonstrate the EO tuning, V_g changes from 0 to 16 V, and the corresponding E_F changes from 0 to 0.75 eV.

The propagation length (L_p), normalized mode field area (A), and figure of merit (FoM) are used to evaluate the performances of the GTDLSPP rib waveguide. L_p is defined as the distance where the initial electromagnetic energy of the guided mode decreases to $1/e$ [40]

$$L_p = \lambda/4\pi \text{Im}(n_{eff}), \quad (5)$$

where n_{eff} is the mode effective RI of the GTDLSPP rib waveguide, Im(n_{eff}) is the imaginary part of n_{eff}.

The effective mode field area A_{eff} is used to describe the energy confinement, which is defined as the ratio of the total electromagnetic energy to the peak energy density of the guided mode [40]

$$A_{eff} = \frac{\iint W(x, y)dxdy}{\max(W(x, y))}. \quad (6)$$

In Eq. (6), $W(x, y)$ and max($W(x, y)$) represent the total electromagnetic energy density distribution of the guided mode and the corresponding peak energy, respectively. In order to evaluate the waveguide performance for guiding light beyond the diffraction limit, the normalized mode field area ($A = A_{eff}/A_0$) is used. Here, $A_0 = \lambda^2/4$ is the diffraction limit mode field area.

To compare the performances of the different waveguides, FoM is defined as the ratio of the propagation distance to the mode field diameter [41]

$$FoM = L_p/(2\sqrt{A/\pi}). \quad (7)$$

The propagation loss of the GTDLSPP rib waveguide is defined as following [30]

$$\alpha_{loss} = \frac{40\pi}{\lambda \ln 10}\text{Im}(n_{eff}) \text{ (dB/μm)}. \quad (8)$$

To analyze the mode characteristics of the GTDLSPP rib waveguide, the commercial COMSOL Multiphysics software based on the finite element method (FEM) is employed. The scattering bound condition is used. To ensure good convergence of the calculated results, the maximum grid sizes for the coated graphene layer and TDLSPP rib waveguide are set as 0.1 nm and 0.08 μm, respectively.

III. WAVEGUIDE CHARACTERISTICS

In this work, $\lambda = 1.55$ μm, $h_3 = 50$ nm, h_2, h_1, and V_g are selected as the sweep parameters. The complex effective RIs of the four hybrid plasmonic modes (HPMs) in the GTDLSPP rib waveguide are calculated. The RI real parts Re (n_{eff}) of the four HPMs with different h_2 and h_1 at a fixed V_G of 3.182 V are shown in Fig. 2(a). Both the mode number and Re (n_{eff}) increase with h_1 when h_2 remains unchanged. For the HPM 1 and HPM 4, Re (n_{eff}) increases with h_2 when h_1 remains unchanged. However, Re (n_{eff}) increases and then decreases with h_2 when h_1 changes from 50 to 250 nm. In order to ensure that the four HPMs are propagated inside the GTDLSPP rib waveguide, h_1 is chosen as 250 nm. To understand the influences of λ, the relationships between Re

(n_{eff}) and λ are shown in Fig. 2(b). From Fig. 2(b), Re (n_{eff}) decreases with the increase of λ for the four HPMs.

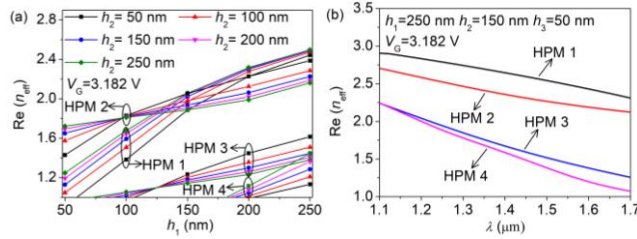**FIGURE 2.** The calculated Re(n_{eff}) of the four HPMs in the GTDLSPP rib waveguide for the different parameters, (a) h_1 and h_2, and (b) λ.

Figs. 3(a)-3(d) show the influences of V_G on Re (n_{eff}) of the four HPMs when h_2=150 nm. The insets in Figs. 3(a)-3(d) show the electric field distributions of the HPM 1, HPM 2, HPM 3, and HPM 4. From Figs. 3(a)-3(d), Re (n_{eff}) has a maximum peak at V_G=~3.2 V which is marked as a red star, and has a smaller peak at V_G= ~8.2 V which is marked as a red dot. The reason for the maximum peak is that Re (n_{eff}) of the monolayer graphene has a maximum value at V_G=~3.2 V. However, Re (n_{eff}) of the monolayer graphene permittivity is nearly zero at V_G=~7.8V, which causes the smaller peak at V_G= ~8.2 V.

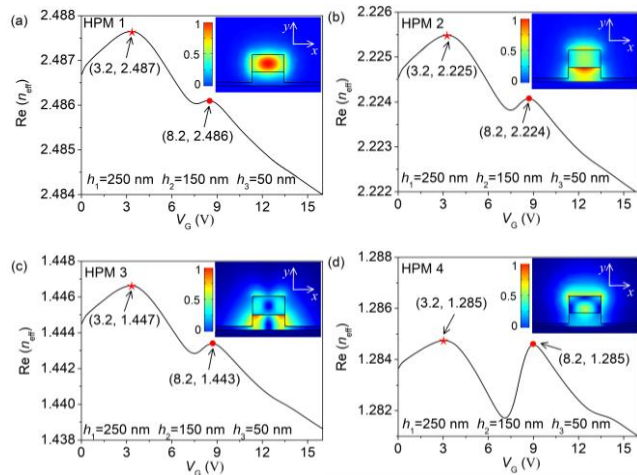**FIGURE 3.** Re (n_{eff}) of (a) HPM 1, (b) HPM 2, (c) HPM 3, and (d) HPM 4 in the GTDLSPP rib waveguide, the insets showing the electric field distributions of the four HPMs.

As shown in the inset of Fig. 3(a), the HPM 1 is a photonic-like mode. The electric field direction of the HPM 1 is along the *x*-axis, and the corresponding electric field energy is mainly concentrated in the upper Si layer. In the inset of Fig. 3(b), the HPM 2 is a conventional HPM, which is generated by a TM mode. Hence, the electric field direction of the HPM 2 is along the *y*-axis, and the electric field energy is mainly concentrated in the middle silicon nitride layer. In the insets of Figs. 3(c) and 3(d), the HPM 3 and HPM 4 are the higher-order HPMs excited by TM modes.

Figs. 4(a) and 4(b) show the propagation length L_p and normalized effective mode field area A of the four HPMs as

functions of V_G when h_1=250 nm, h_2=150 nm, and h_3=50 nm. In Fig. 4(a), L_p of HPM 1, HPM 2, and HPM 3 have the large peaks at V_G of 13.8, 1.6, and 3.6 V. Moreover, L_p of the HPM 1, HPM 2, and HPM 3 can achieve 10^3, 10^2, and 10 mm-scale, respectively, which is longer than that of a conventional TDLSPP waveguide. For the HPM 4, there is only a smaller peak at V_G of 8.2 V. L_p is ~10^2 μm, which is comparable to that of a TDLSPP waveguide. A of the four HPMs are shown in Fig. 4(b). It can be seen from Fig. 4(b) that A of the HPM 1 has little change with V_G. As a photonic-like mode, the mode field distribution of the HPM 1 hardly changes with the monolayer graphene. However, A of the HPM 2, HPM 3, and HPM 4 change significantly when V_G goes up to a certain value. There is a minimum when V_G is ~13.8 V (E_F=~0.75 eV). To explain the reasons for the changes, the real and imaginary parts Re (n_g) and Im (n_g) of the refractive index n_g of the graphene are shown in Fig. 4(c). From Fig. 4(c), Re (n_g) is larger than Im (n_g) when V_G is lower than 8 V. The guided mode plays a dominant role in the HPM, which result in a larger A. However, Im (n_g) becomes larger than Re (n_g) when V_G is higher than 8 V. The monolayer graphene is close to a very thin "metal" layer [37]. The SPP mode plays an important role in the HPM, which can improve the field confinement of the GTDLSPP rib waveguide. When V_G increase to ~13 V, Re (n_g) reduces to less than 0.1, and Im (n_g) increases to larger than 1.5. The ohmic loss increases due to the enhanced metallic property of the graphene, which reduces the field distribution ratio in the core of the GTDLSPP rib waveguide and makes A larger. The normalized A_{ef} of ~0.010, ~0.003, and ~0.012 for the HPM 2, HPM 3, and HPM 4 are achieved. That is, A_{eff} of the HPM 2, HPM 3, and HPM 4 are ~λ^2/400, ~λ^2/1333, and ~λ^2/333, respectively.
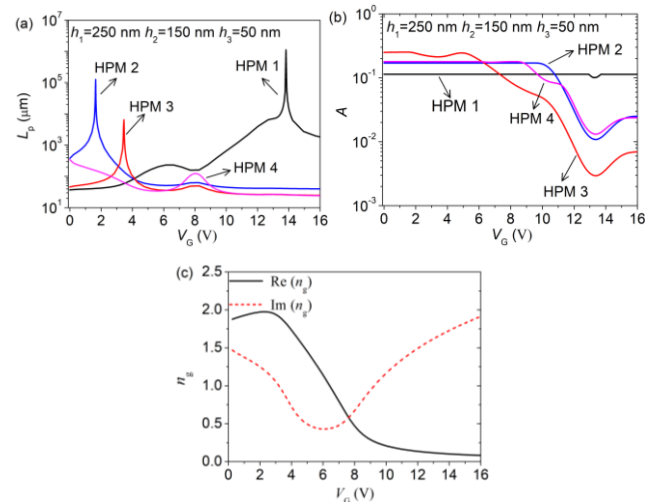

FIGURE 4. Mode characteristics of the four HPMs as functions of V_G when h_1 =250 nm, h_2=150 nm, and h_3 =50 nm, (a) the propagation length L_p, (b) the normalized mode field area A, and (c) the refractive index n_g of the monolayer graphene.

TABLE 1
MODE CHARACTERISTICS OF THE GTDLSPP RIB WAVEGUIDE AND TDLSPP RIB WAVEGUIDE

Modes	GTDLSPP Rib Waveguide				TDLSPP Rib Waveguide (without graphene)		
	L_p (µm)	A	FoM	V_G (V)	L_p (µm)	A	FoM
HPM 1	1.11×10^6	0.101	2.13×10^6	13.8	429.88	0.114	821.4159
HPM 2	1.26×10^5	0.170	1.98×10^5	1.6	37.28	0.170	58.33373
HPM 3	6.54×10^3	0.213	9.14×10^3	3.5	22.55	0.146	38.07487
HPM 4	137.37	0.179	309.39	8.3	22.22	0.115	42.27304

To illustrate the effect of graphene, the mode characteristics of the GTDLSPP rib waveguide and TDLSPP rib waveguide are listed in Table 1 for comparison. L_p and FoMs of the GTDLSPP rib waveguide are much better than those of the TDLSPP waveguide.

In order to optimize the structure parameters of the GTDLSPP rib waveguide, FoM is investigated when h_1 and h_2 are changed. The maximum values of FoM (max (FoM)) with different h_1 and h_2 are shown in Figs. 5(a)-5(d). The influences of h_1 and h_2 on the max (FoM) for the HPM 1 are greater than those for the HPM 2 and HPM 3 when $h_1 < 200$ nm. For the HPM 2 and HPM 3, the max (FoM) changes significantly with h_2 when $h_1 = 250$ nm. The max (FoM) of the HPM 4 changes slowly because the max (FoM) mainly depends on A_{eff} which has a minimum at $V_G = 13.8$ V. Considering the tradeoff between the four HPMs, h_1 and h_2 are chosen as 250 and 150 nm, respectively. At this time, the max (FoM) of ~10^6 for the HPM 1, ~10^5 for the HPM 2, ~10^4 for the HPM 3, and ~10^2 for the HPM 4 are achieved.
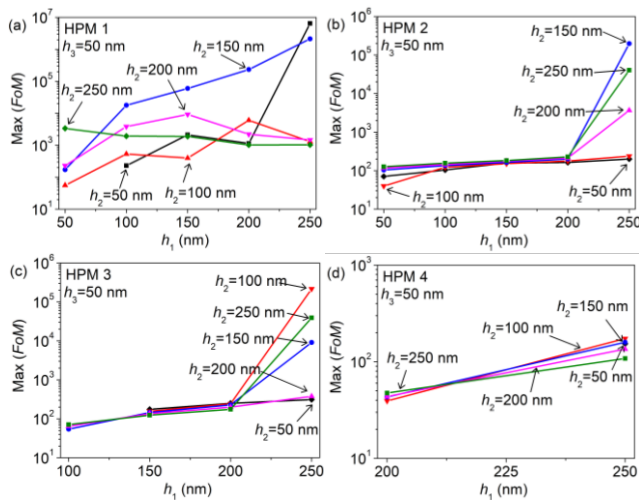

FIGURE 5. Maximum values of *FoMs* (max (*FoM*)) with the different h_1 and h_2 for the (a) HPM 1, (b) HPM 2, (c) HPM 3, and (d) HPM 4.

IV. THE EO MODULATION PERFORMANCES

The Au electrode is deposited directly above the GTDLSPP rib waveguide, as shown in Fig. 1(a), and Au slab under the rib waveguide is used as another electrode. The bias voltage V_G can be changed by applying the static electric potential across the Au electrodes. Fig. 6 shows the propagation loss (α_{loss}) spectra of the four HPMs for the different V_G. For

comparison, α_{loss} spectra of the TDLSPP rib waveguide (without graphene) are also shown in Figs. 6(a)-6(d). λ changes from 1.4 to 2.4 µm for the HPM 1, and from 1.1 to 1.7 µm for the HPM 2, HPM 3, and HPM 4. There is only one peak for the HPM 1, HPM 2, and HPM 3. However, there are two peaks for the HPM 4. To show the EO tuning of the designed GTDLSPP rib waveguide, the range of V_G changes between 0 and 10.4 V. The loss peaks of the HPM 1, HPM 2, and HPM 3 and peak 2 of the HPM 4 are blue-shifted when V_G changes from 0 to 10.4 V. However, the peak 1 of the HPM 4 changes slowly.
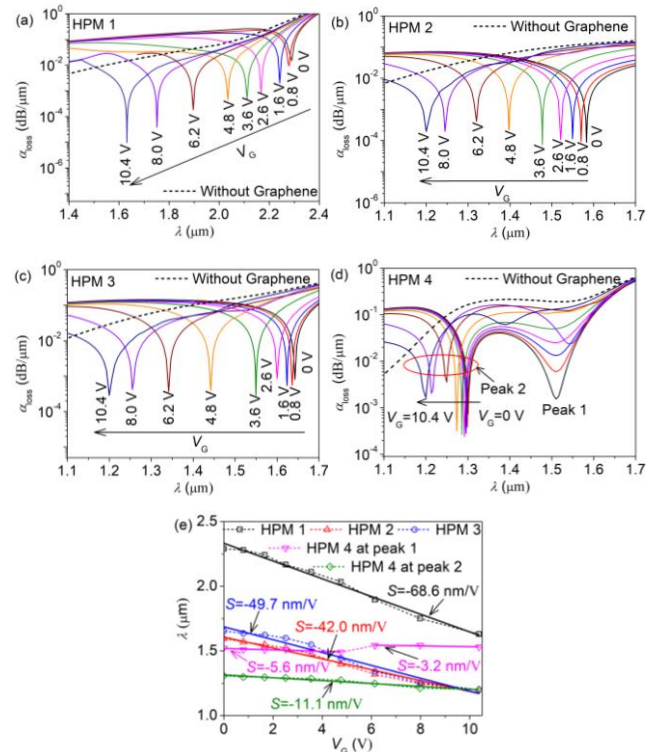
FIGURE 6. The loss spectra of the four HPMs: (a) HPM 1, (b) HPM 2, (c) HPM 3, (d) HPM 4, and (e) the EO wavelength tunings and linear fittings.

The wavelength changes of the peaks in the loss spectra with V_G and the linear fittings are shown in Fig. 6(e). The EO modulation of the GTDLSPP rib waveguide is achieved in large wavelength ranges from 1.5 to 2.3 µm for the HPM 1, and 1.2 to 1.65 µm for the other HPMs. The EO wavelength tuning (EOWT) can be obtained by the slopes (S) of the fitting lines. The linear fitting results of the four HPMs are

listed in Table 2. The EOWTs of -68.2, -42.0, and -49.7 nm/V are achieved for the HPM 1, HPM 2, and HPM 3. For the peak 2 of the HPM 4, the EOWT is -11.1 nm/V. Moreover, the EOWTs of the HPM 1, HPM 2, HPM 3, and peak 2 of the HPM 4 have good linearity when V_G is changed from 0 to 10.4 V. However, the peak 1 of the HPM 4 shows the piecewise linearity. The EOWTs are -5.6 and -3.2 nm/V when V_G changes from 0 to 4.8 V and 6.2 to 10.4 V, respectively.

The EOWTs of several other modulators are also listed in Table 2 for comparison. From Table 2, the EOWTs of the GTDLSPP rib waveguide are two orders of magnitude higher than that of other structures.

TABLE 2
THE EO WAVELENGTH TUNINGS FOR THE FOUR HPMS IN THE DESIGNED GTDLSPP RIB WAVEGUIDE AND SEVERAL OTHER STRUCTURES REPORTED

Configurations	*EOWT*	Standard Error (nm/V)	Determination coefficient R^2	Refs.
HPM 1	-68.6 nm/V	2.78	0.987	this work
HPM 2	-42.0 nm/V	2.31	0.976	
HPM 3	-49.7 nm/V	3.53	0.961	
Peak 1 of HPM 4	-5.6 nm/V	1.05	0.843	
	-3.2 nm/V	1.71	0.875	
Peak 2 of HPM 4	-11.1 nm/V	0.91	0.949	
LNOI microring	3 pm/V	-	-	[42]
SOI ring	26 pm/V	-	-	[43]
AlN microring	0.18 pm/V	-	-	[44]
Silicon racetrack	28 pm/V			[45]

To show the propagation characteristics of the HPMs in the GTDLSPP rib waveguide, L_G is set as 150 μm. The transmission spectra of the four HPMs with different V_G are shown in Figs. 7(a)-7(d). It can be seen from Figs. 7(a)-7(c) that for the HPM 1, HPM 2, and HPM 3, the large peaks emerge at a fixed V_G. The wavelengths of the peaks have distinct blue-shifts and the widths of the peaks enlarge when V_G increases. However, there are two peaks at wavelengths ~1.3 and ~1.5 μm for the HPM 4, as shown in Fig. 7(d). The peak 1 drops rapidly when V_G is larger than 4 V. The width of the peak 2 hardly changes when $V_G < 4$ V, and the peak wavelength slightly occurs to blue-shift when $V_G > 4$ V.
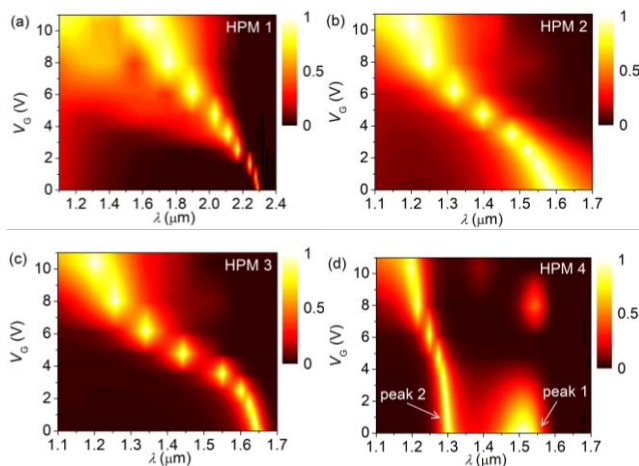

FIGURE 7. The transmission spectra of the GTDLSPP rib waveguide with different V_G and $λ$, (a) HPM 1, (b) HPM 2, (c) HPM 3, and (d) HPM 4.

In order to evaluate the modulation performances, the normalized transmission spectra of the four HPMs are shown in Figs. 8(a)-8(d) when V_G=0.8, 3.6, 4.8, and 10.4 V,

respectively, and L_G=150 μm. Moreover, the modulation depth (M) is defined as

$$M = 1 - \frac{T_{min}}{T_{max}} \quad \text{or} \quad ME \text{ (dB)} = 10\log_{10}(\frac{T_{max}}{T_{min}}) = -10\log_{10}(1-M),$$
(9)

where T_{max} and T_{min} are the maximum and minimum of the transmission spectra, corresponding to the "ON" and "OFF" states, respectively. Here, the "OFF" or "ON" state of the modulators means that the light is blocked or not blocked, and the gate voltages at the "ON" and "OFF" states are represented by V_{ON} and V_{OFF}, respectively. ME (dB) is another representation of the modulation depth. In Fig. 8(a), V_{ON} and V_{OFF} for the HPM 1 are chosen as 10.4 and 0.8 V, respectively. The full-width at half-maximum (FWHM) of the peak for the "ON" state is ~450 nm when the wavelength ($λ_{on}$) at the "ON" state is ~1.64 μm. At this time, M is ~98.7%. It will slightly drop when V_{OFF} increases from 0.8 to 4.8 V. In Figs. 8(b) and 8(c), for the HPM 2 and HPM 3, V_{ON} and V_{OFF} are chosen as 3.6 and 10.4 V, respectively. M of ~87.9% and FWHM of ~100 nm are obtained for the HPM 2 when $λ_{on}$=~1.48 μm. M of ~99.5% and FWHM of ~42 nm are obtained for the HPM 3 when $λ_{on}$=~1.55 μm. In Fig. 8(d), V_{ON} and V_{OFF} are 0.8 and 4.8 V for the peak 1 at ~1.51 μm, and are reversed for the peak 2 at ~1.28 μm. M of ~97.3 and ~75.2% and FWHMs of ~92 and ~34 nm are achieved for the peak 1 and peak 2. With the increase of V_{OFF}, M will be greatly improved for the peak 2. To show the effect of L_G on the modulation performance, the changes of M and FWHM with the increase of L_G are shown in Fig. 8(e). When L_G changes from 0.5 to 300 μm, M increases sharply and then approaches to the saturation, while FWHM decreases

gradually. The FWHM of the transmission peak is out of the considered wavelength range when L_G<50 nm. The insertion losses (*IL*s) for the different L_G are calculated by $IL(dB) = -10\log_{10}(T_{max})$, as shown in Fig. 8(f). *IL*s for the four HPMs increase when L_G increases from 0.5 to 300 μm. When L_G is less than 150 μm, *IL*s are lower than 6 dB. *IL*s of ~0.05 and 1.01 dB are achieved for the HPM 1 and HPM 2, respectively. Considering a compromise of *M*, FWHM, and *IL*, L_G=150 μm is the optimum value.
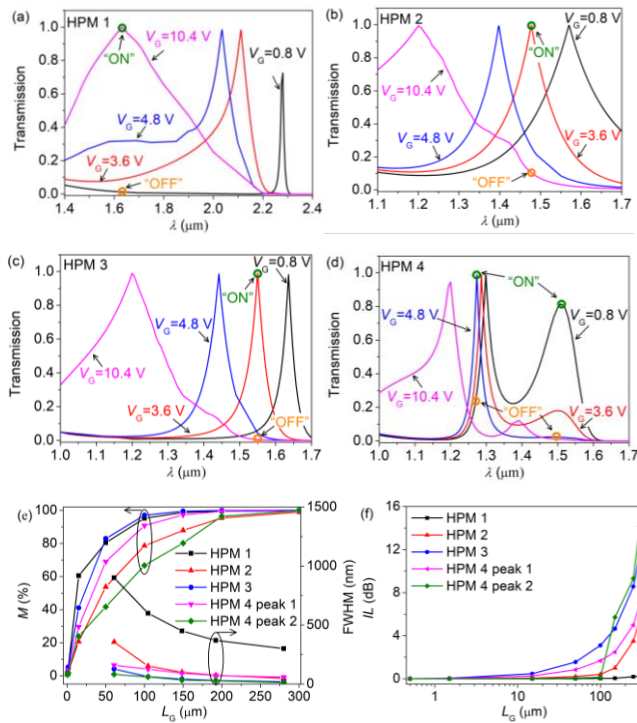

FIGURE 8. The transmission spectra of (a) HPM 1, (b) HPM 2, (c) HPM 3, and (d) HPM 4 in the GTDLSPP rib waveguide when L_G=150 μm, (e) *M* and FWHM, and (f) *IL* as functions of L_G.

The normalized electric field distributions of the "ON" and "OFF" states in the *xy* plane and the major components in the *xz* and *yz* planes for the four HPMs in the GTDLSPP rib waveguide are shown in Figs. 9(a)-9(e). The major component of the electric field is E_x for the HPM 1, and E_y for the HPM 2, HPM 3, and HPM 4. From Figs. 9(a)-9(e), the normalized electric field distributions of the "ON" and "OFF" states indicate that most of the light energy can or not pass through the GTDLSPP rib waveguide.

Table 3 shows the related parameters, including *M*, *IL*, λ_{on}, FWHM of the peaks at λ_{on}, voltage difference between V_{ON} and V_{OFF} ($\Delta V_G=V_{ON}-V_{OFF}$), and E_F in "on" and "OFF" states (E_F (ON) and E_F (OFF)). The modulation performances of some different on-chip EO modulators are listed in Table 4 for comparison. From Table 4, *M* and *IL* of the EO modulator based on the designed GTDLSPP rib waveguide is comparable or superior to those of other structures, while the bandwidth is larger than those of other structures.
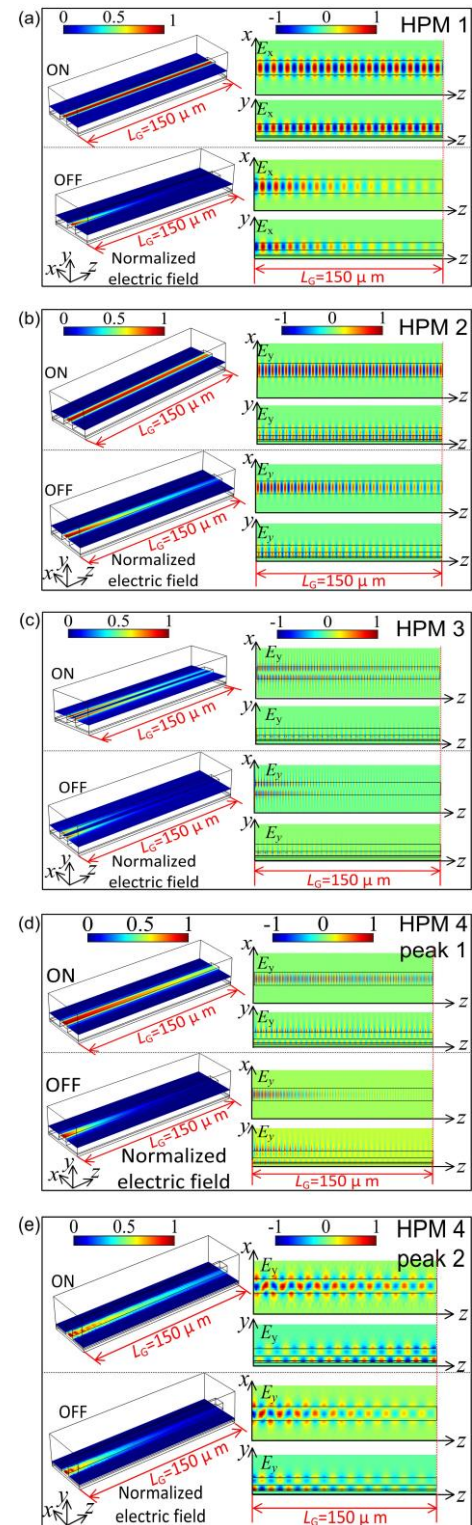

FIGURE 9. Electric field distributions of (a) HPM 1, (b) HPM 2, (c) HPM 3, (d) peak 1 of HPM 4, and (e) peak 2 of HPM 4 when L_G=150 μm.

V. Conclusions

In summary, we propose a GTDLSPP rib waveguide. The simulation results show that the GTDLSPP rib waveguide can achieve a 10^3 mm-scale propagation length and a max

(*FoM*) of ~10^6. A high EO wavelength tuning of -68.6 nm/V is also achieved. The proposed GTDLSPP rib waveguide provides a feasible scheme for the EO amplitude modulation in a wide wavelength range from 1.2 to 2.4 µm. Considering the tradeoff between M and FWHM, M of ~98.7% and FWHM of ~450 nm are achieved for a 150-µm long GTDLSPP rib waveguide by changing V_G.

The GTDLSPP rib waveguide could provide a feasible on-off keying scheme for the on-chip EO modulation, along with compact footprint, high modulation depth, and broad bandwidth. It also has the promising applications in the EO tunable devices, optical interconnects, and optical switches due to the high EO wavelength tuning. Moreover, the silicon nitride has good optical characteristics in the mid-infrared spectral region, so the proposed GTDLSPP waveguide can also find application in the mid-infrared optoelectronic devices. At the same time, the biocompatibility of the graphene makes the GTDLSPP waveguide convenient for the biochemical sensing.

TABLE 3
MODULATION PERFORMANCES OF THE DESIGNED GTDLSPP RIB WAVEGUIDE

Mode	M	ME (dB)	IL (dB)	λ_{on} (µm)	FWHM (nm)	ΔV_G (V)	E_F (ON) (eV)	E_F (OFF) (eV)
HPM 1	98.7%	18.9	~0.05	1.64	450	9.6	0.65	0.18
HPM 2	87.9%	9.2	~1.01	1.48	100	-6.8	0.38	0.65
HPM 3	99.5%	23.0	~4.65	1.55	42	-6.8	0.38	0.65
Peak 1 of HPM 4	97.3%	15.8	~2.49	1.51	92	-4	0.18	0.44
Peak 2 of HPM 4	75.2%	6.0	~5.71	1.28	34	4	0.44	0.18

TABLE 4
MODULATION PERFORMANCES OF SOME DIFFERENT STRUCTURES REPORTED

Structure	M	ME (dB)	IL (dB)	Length	λ_{on} (µm)	FWHM (nm)	f_{3dB} (GHz)	ΔV_G (V)	Refs.
Hybrid graphene silicon waveguide	-	>20	0.23	20 µm	1.55	>300	-	-	[3]
All-optical graphene SPP structure	-	114.7 dB/µm	-	-	7.634	-	-	1.16	[6]
Graphene-silicon microring resonator	12.5%	-	-	50 µm radius	~1.555	-	-	8.8	[12]
Graphene-integrated FP microcavity	90%	-	-	-	33.16 THz	-	-	-	[13]
Periodic metasurfaces	94.96	-	-	-	1.55	-	0.630	9.6	[14]
Groove metasurface with graphene.	-	0.4 dB/µm	0.0056 dB/µm	-	1.55	300	-	3.9	[15]
Graphene-on-Silicon slot waveguide	~28 dB	0.283 dB/µm	1.28	120 µm	1.55	0.96	117	1.32	[19]
Silver nanowire on Si-Graphene-SiO$_2$	-	0.6 dB/µm	0.05 dB/µm	-	1.55	-	-	-	[26]
MZI and microring resonator	5.5 dB		1.9	740 nm	1.55	-	83.4	-	[28]
Graphene-based plasmonic valley-slot waveguide	3dB	10.4 dB/µm	<4 dB/µm	290 nm	1.55	~200	-	0.95	[29]
Graphene-hBN-graphene waveguide	39.75%	13.75 dB/µm	-		1.55	-	190.5	3.13	[30]
Ultra-thin silicon strip waveguide with graphene	-	0.297 dB/µm	~0.015 dB/µm	150 µm	1.31	-	72	3.07	[32]
		0.304 dB/µm			1.55				
		0.306 dB/µm			2.00				
Graphene-Si$_3$N$_4$ waveguide	-	0.166 dB/µm	~0.017 dB/µm	18.09 µm	1.55	-	-	3.82	[34]
Planar Fabry–Pérot microcavity	80%	-	-	18.097 µm	1.55	0.408	-	5.87	[46]

REFERENCES

[1] S. Richard, "The past, present, and future of silicon photonics," IEEE J. Sel. Top. Quant., vol. 12, no. 6, pp. 1678-1687, Nov. 2006.

[2] J. D. Cox, and F. J. García de Abajo, "Single-plasmon thermo-optical switching in graphene," Nano Lett., vol. 19, no. 6, pp. 3743-3750, May 2019.

[3] Y. Xu, F. Li, Z. Kang, D. Huang, X. Zhang, H. Tam, and K. A. P. Wai, "Hybrid graphene-silicon based polarization-insensitive electro-absorption modulator with high-modulation efficiency and ultra-broad bandwidth," Nanomaterials, vol. 9, no. 2, p. 157, Jan. 2019.

[4] V. V. Temnov, G. Armelles, U. Woggon, D. Guzatov, A. Cebollada, A. Garcia-Martin, J. Garcia-Martin, T. Thomay, A. Leitenstorfer, and R. Bratschitsch, "Active magneto-plasmonics in hybrid metal–ferromagnet structures," Nat. Photonics, vol. 4, pp. 107-111, Feb. 2010.

[5] A. Pianelli, R. Kowerdziej, M. Dudek, K. Sielezin, M. Olifierczuk, and J. Parka, "Graphene-based hyperbolic metamaterial as a switchable reflection modulator," Opt. Express, vol. 28, no. 5, pp. 6708-6718, Mar. 2020.

[6] L. Yang, C. Pei, A. Shen, C. Zhao, Y. Li, X. Li, H. Yu, Y. Li, X. Jiang, and J. Yang, "An all-optical modulation method in sub-micron scale," Sci. Rep., vo 5, p. 9206, Mar. 2015.

[7] K. S. Novoselov, A. K. Geim, S. V. Morozov, D. Jiang, M. I. Katsnelson, I. V. Grigorieva, S. V. Dubonos, and A. A. Firsov, "Two-dimensional gas of massless Dirac fermions in graphene," Nature, vol. 438, pp. 197-200, Nov. 2005.

[8] F. Wang, Y. Zhang, C. Tian, C. Girit, A. Zettl, M. Crommie, and Y. R. Shen, "Gate-variable optical transitions in graphene," Science, vol. 320, no. 5873, pp. 206-209, Apr. 2008.

[9] G. T. Reed, G. Mashanovich, F. Y. Gardes, and D. J. Thomson, "Silicon optical modulators," Nat. Photonics, vol. 4, pp. 518-526, Jul. 2010.

[10] S. Luo, Y. Wang, X. Tong, and Z. Wang, "Graphene-based optical modulators," Nanoscale Res. Lett., vol. 10, p. 199, Apr. 2015.

[11] H. Shu, Z. Su, L. Huang, Z. Wu, X. Wang, Z. Zhang, and Z. Zhou, "Significantly high modulation efficiency of compact graphene modulator based on silicon waveguide," Sci. Rep., vol. 8, p. 991 Jan. 2018.

[12] Y. Ding, X. Zhu, S. Xiao, H. Hu, L. H. Frandsen, N. A. Mortensen, and K. Yvind, "Effective electro-optical modulation with high Extinction ratio by a graphene-silicon microring resonator," Nano Lett., vol. 15, no. 7, pp. 4393-4400, Jun. 2015.

[13] C. Zeng, J. Guo, and X. Liu, "High-contrast electro-optic modulation of spatial light induced by graphene-integrated Fabry-Pérot microcavity," Appl. Phys. Lett., vol. 105, p. 121103, Sep. 2014.

[14] S. Bahadori-Haghighi, R. Ghayour, and M. H. Sheikhi, "Double-layer graphene optical modulators based on Fano resonance in all-dielectric metasurfaces," J. Appl. Phys., vol. 125, p. 073104, Feb. 2019.

[15] Y. Wang, T. Li, and S. Zhu, "Graphene-based plasmonic modulator on a groove-structured metasurface," Opt. Lett., vol. 42, no. 12, pp. 2247-2250, Jun. 2017.

[16] J. Shin, and J. T. Kim, "Broadband silicon optical modulator using a graphene-integrated hybrid plasmonic waveguide," Nanotechnology, vol. 26, no. 36, p. 365201, Aug. 2015.

[17] C. T. Phare, Y. Daniel Lee, J. Cardenas, and M. Lipson, "Graphene electro-optic modulator with 30 GHz bandwidth," Nat. Photonics, vol. 9, pp. 511-514, Jul. 2015.

[18] M. Liu, X. Yin, E. Ulin-Avila, B. Geng, T. Zentgraf, L. Ju, F. Wang, and X. Zhang, "A graphene-based broadband optical modulator," Nature, vol. 474, pp. 64-67, Jun. 2011.

[19] J. L, Z. D, X. Y, G. Y, W. C, W. X, L. Z, and S. X, "Design of an Electro-absorption modulator based on graphene-on-silicon slot waveguide," IEEE Photonics J., vol. 11, no. 3, p. 7800911, JUN. 2019.

[20] Y. Fang, and M. Sun, "Nanoplasmonic waveguides: towards applications in integrated nanophotonic circuits," Light-Sci. Appl., vol. 4, p e294, Jun. 2015.

[21] W. L. Barnes, A. Dereux, and T. W. Ebbesen, "Surface plasmon subwavelength optics," Nature, vol. 424, pp. 824-830, Aug. 2003.

[22] M. Z. Alam, J. S. Aitchison, and M. Mojahedi, "A marriage of convenience: Hybridization of surface plasmon and dielectric waveguide modes," Laser Photonics Rev., vol. 8, pp. 394-408, Feb. 2014.

[23] I. A. Pshenichnyuk, G. I. Nazarikov, S. S. Kosolobov, A. I. Maimistov, and V. P. Drachev, "Edge-plasmon assisted electro-optical modulator," Phys. Rev. B, vol. 100, p. 95434, Nov. 2019.

[24] J. Gosciniak, and D. T. H. Tan, "Graphene-based waveguide integrated dielectric-loaded plasmonic electro-absorption modulators," Nanotechnology, vol. 24, p. 185202, Apr. 2013.

[25] W. Gao, J. Shu, C. Qiu, and Q. Xu, "Excitation of plasmonic waves in graphene by guided-mode resonances," ACS Nano, vol. 6, no. 9, pp. 7806-7813, Aug. 2012.

[26] S. Qu, C. Ma, and H. Liu, "Tunable graphene-based hybrid plasmonic modulators for subwavelength confinement," Sci. Rep., vol. 7, p. 5190, Jul. 2017.

[27] F. C. Ni, Z. T. Xie, X. Hu, C. Jia, and X. G. Huang, "Selective Angular Momentum Generator Based on a Graphene Hybrid Plasmonic Waveguide," J. Lightwave Technol., vol. 37, no. 21, pp. 5486-5492, Nov. 2019.

[28] J. Luan, P. Zheng, H. Yang, G. Hu, R. Zhang, B. Yun, and Y. Cui, "A Compact Graphene Modulator Based on Localized Surface Plasmon Resonance with a Chain of Metal Disks," Plasmonics, vol. 14, pp. 1949-1954, Dec. 2019.

[29] M. Shirdel, and M. A. Mansouri-Birjandi, "A broadband graphene modulator based on plasmonic valley-slot waveguide," Opt. Quant. Electron., vol. 52, p. 36, Dec. 2020.

[30] X. Chen, Y. Wang, Y. Xiang, G. Jiang, L. Wang, Q. Bao, H. Zhang, Y. Liu, S. Wen, and D. Fan, "A Broadband Optical Modulator Based on a Graphene Hybrid Plasmonic Waveguide," J. Lightwave Technol., vol. 34, no. 12, pp. 4948-4953, Nov. 2016.

[31] H. Vahed, and S. S. Ahmadi, "Graphene-based plasmonic electro-optic modulator with sub-wavelength thickness and improved modulation depth," Appl. Phys. B, vol. 123, p. 265, Oct. 2017.

[32] X. Hu, Y. Zhang, D. Chen, X. Xiao, and S. Y "Design and Modeling of High Efficiency Graphene Intensity/Phase Modulator Based on Ultra-Thin Silicon Strip Waveguide," J. Lightwave Technol., vol. 37, no. 10, pp. 2284-2292, May 2019.

[33] J. F. Bauters, M. J. R. Heck, D. D. John, J. S. Barton, C. M. Bruinink, A. Leinse, R. G. Heideman, D. J. Blumenthal, and J. E. Bowers, "Planar waveguides with less than 0.1 dB/m propagation loss fabricated with wafer bonding," Opt. Express, vol. 19, no. 24, pp. 24090-24101, Nov. 2011.

[34] M. Fan, H. Yang, P. Zheng, G. Hu, B. Yun, and Y. Cui, "Multilayer graphene electro-absorption optical modulator based on double-stripe silicon nitride waveguide," Opt. Express, vol. 25, no. 18, pp. 21619-21629, Sep. 2017.

[35] H. Lu, B. P. Cumming, and M. Gu, "Highly efficient plasmonic enhancement of graphene absorption at telecommunication wavelengths," Opt. Lett., vol. 40, No. 15, pp. 3647-3650, Aug. 2015.

[36] P. B. Johnson, and R. W. Christy, "Optical constants of the noble metals," Phys. Rev. B, vol. 6, no. 12, pp. 4370-4379, Dec. 1972.

[37] A. Vakil, and N. Engheta, "Transformation optics using graphene," Science, vol. 332, no. 6035, pp. 1291-1294, Jun. 2011.

[38] B. Zhao, J. M. Zhao, and Z. M. Zhang, "Enhancement of near-infrared absorption in graphene with metal gratings," Appl. Phys. Lett., vol. 105, no. 3, p. 031905, Jul. 2014.

[39] F. Valmorra, G. Scalari, C. Maissen, W. Fu, C. Schönenberger, J. W. Choi, H. G. Park, M. Beck, and J. Faist, "Low-bias active control of terahertz waves by coupling large-area CVD graphene to a terahertz metamaterial," Nano Lett., vol. 13, no. 7, 3193-3198, Jun. 2013.

[40] K. Zheng, Y. Yuan, J. He, G. Gu, F. Zhang, Y. Chen, J. Song, and J. Qu, "Ultra-high light confinement and ultra-long propagation distance design for integratable optical chips based on plasmonic technology," Nanoscale, vol. 11, pp. 4601-4613, Feb. 2019.

[41] P. Berini, "Figures of merit for surface plasmon waveguides," Opt. Express, vol.14, no. 26, pp. 13030-13042, Dec. 2006.

[42] I. Krasnokutska, J. J. Tambasco, and A. Peruzzo, "Tunable large free spectral range microring resonators in lithium niobate on insulator," Sci. Rep., vol.9, p. 11086, Jul. 2019.

[43] G. Li, X. Zheng, J. Yao, H. Thacker, I. Shubin, Y. Luo, K. Raj, J. E. Cunningham, and A. V. Krishnamoorthy, "25Gb/s 1V-driving

This article has been accepted for publication in a future issue of this journal, but has not been fully edited. Content may change prior to final publication. Citation information: DOI 10.1109/ACCESS.2020.2999395, IEEE Access

IEEE Access

T. Ma et al.: GTDLSPP rib waveguide for electro-optic modulation

CMOS ring modulator with integrated thermal tuning," Opt. Express, vol. 19, no. 21, pp. 20435-20443, Oct. 2011.

[44] H. Jung, K. Y. Fong, C. Xiong, and H. X. Tang, "Electrical tuning and switching of an optical frequency comb generated in aluminum nitride microring resonators," Opt. Lett., vol. 39, no. 1, pp. 84-87, Jan. 2014.

[45] H. Yu, M. Pantouvaki, S. Dwivedi, P. Verheyen, G. Lepage, R. Baets, W. Bogaerts, P. Absil, and J. V. Campenhout, "Compact thermally tunable silicon racetrack modulators based on an asymmetric waveguide," IEEE Photon. Technol. Lett., vol. 25, no. 2, pp. 159-162, Jan. 2013.

[46] C. A. Barrios, V. R. de Almeida, M. Lipson, "Low-power-consumption short-length and high-modulation-depth silicon electrooptic modulator," J. Lightwave Technol., vol. 21, no. 4, pp. 1089-1098, Apr. 2003.

Heng Liu received the B.S. degree in information and computing science from Henan Normal University, Xinxiang, China, in 2001 and the M. S. degree in computer software and theory from Shanghai Maritime University, Shanghai, China, in 2006. Her current research interests include pattern recognition, image retrieval and computer aided modeling.

Tao Ma received the PhD degree in optical engineering from Beijing University of Posts and Telecommunications, Beijing, China, in 2017 and the M.S. degree in electronic and information engineering from microelectronics and solid-state electronics from South China Normal University, Guangzhou, China, in 2005. His current research interests include electromagnetic metamaterial, micro-nano ring resonance, optoelectronic device and optical sensing.

Xian Zhou received the Ph.D. degree in electromagnetic field and microwave technology from Beijing University of Posts and Telecommunications (BUPT), Beijing, China, in 2011. She is currently an Associate Professor at the Department of computer and communication engineering, University of Science and Technology Beijing (USTB). She is also a Hong Kong Scholar at the Photonics Research Centre, Department of Electronic and Information Engineering, The Hong Kong Polytechnic University. Her research interests are focused on high-speed optical communications, short reach communications and digital signal processing.

Jinhui Yuan (Senior Member, IEEE) received the Ph.D. degree in physical electronics from the Beijing University of Posts and Telecommunications (BUPT), Beijing, China, in 2011. He is currently a Professor with the Department of Computer and Communication Engineering, University of Science and Technology Beijing (USTB). He was selected as a Hong Kong Scholar at the Photonics Research Center, Department of Electronics and Information Engineering, The Hong Kong Polytechnic University, in 2013. He has published more than 200 articles in the academic journals and conferences. His current research interests include photonic crystal fibers, silicon waveguide, and optical fiber devices. He is the Senior Members of IEEE and OSA.

Keping Long (Senior Member, IEEE) received his M.S. and Ph.D. degrees at UESTC in 1995 and 1998, respectively. He worked as an Associate Professor at Beijing University of Posts and Telecommunications. From July 2001 to November 2002, he was a Research Fellow in the ARC Special Research Centre for Ultra Broadband Information Networks (CUBIN) at the University of Melbourne, Australia. He is now a Professor and Dean at the School of Computer and Communication Engineering, USTB. He is a member of the Editorial Committee of Sciences in China Series F and China Communications. He has also been a TPC and ISC member for COIN, IEEE IWCN, ICON, and APOC, and Organizing Co-Chair of of IWCMC '06, TPC Chair of COIN '05/'08, and TPC Co-Chair of COIN '08/'10. He was awarded the National Science Fund Award for Distinguished Young Scholars of China in 2007 and selected as the Chang Jiang Scholars Program Professor of China in 2008. His research interests are optical Internet technology, new generation network technology, wireless information networks, value-added service, and secure network technology. He has published over 200 papers, 20 keynotes, and invited talks.

Fang Wang received the Ph. D. degree from Henan Normal University in 2016, and received the M.S. in Measurement technology and instruments from the Dalian University of Technology in 2003. From 2016 and then, she was a Professor in the College of Electronic and Electrical Engineering of Henan Normal University. She was a doctoral tutor of optical engineering in the school of Physics. Her current research interests include the photoelectric detection technology, and the design and application research of the optical fiber sensor.

Chongxiu Yu graduated from the Beijing University of Posts and Telecommunications (BUPT), Beijing, China, in 1969. Now he is with the BUPT as a professor. She is engaged in university education and research work and has been the Principal Investigator of many projects supported by China 863 plan, the National Natural Science Foundation and the National Ministry of Science Technology, and so on. Up to now she has published more than 300 papers. Her Research interests are the optical fiber communication, photonic switching, and optoelectronics technology and its applications. Prof. Yu is the Members of Chinese Institute of Communication, Committee of Fiber Optics and Integral Optics, and Chinese Optical Society.

Yufang Liu received the Ph. D. degrees from Dalian University of Technology. He is the member of the National Natural Science Foundation Committee of the thirteenth expert review team. In 2006, he was a doctoral tutor and part-time professor at Beijing Institute of Technology. He is currently a Full Professor with the Henan Normal University, Xinxiang, China. His current research interests include development of fiber-optic sensors and device, Infrared Physics and technology, novel sensor materials and principles, and optical measurement technologies. In the past five years, he has authored or coauthored more than 50 articles in the Phys. Chem. Chem. Phys J., Comput. Chem. Phys., Lett. Phys., Phys. Lett. Chem. and other important academic journals published in more than. He is a member of China Ordnance Industry Association Professional Committee of Optics and the member of Editorial Boards of journals such as the optical technique, Optical Instruments, and Process Automation Instrumentation. Prof. Liu was awarded as the outstanding youth fund of Henan Province in 2004. In 2008, he was awarded as the university outstanding scientific research talent innovation project of Henan Province. From 2006 to 2015, he was awarded by the National Natural Science Foundation of China for four times.